Proceeding *20th SEAGC - 3rd AGSSEA Conference in conjunction with 22nd Annual Indonesian National Conference on Geotechnical Engineering.* Jakarta - INDONESIA, 6 -7 November 2018. ISBN No. 978-602-17221-6-9

# Numerical Simulations of an Excavation Case in Central Jakarta by Hypoplasticity Model for Clays

Melisa Kosasi[1], Fuchen Teng[2], Benson B. C. Hsiung[3]
[1]*Department of Civil and Construction Engineering, National Taiwan Univ. of Science and Technology, Taiwan;*
[2]*Department of Civil and Construction Engineering, National Taiwan Univ. of Science and Technology, Taiwan;*
[3]*Department Civil Engineering, National Kaohsiung Univ. of Science and Technology, Taiwan;*
*E-mail*: melisakosasi9@gmail.com; FTeng@mail.ntust.edu.tw; benson@cc.kuas.edu.tw

**ABSTRACT:** Numerical simulations of a top-down constructed excavation in Central Jakarta was carried out in this study. The excavation supported by the diaphragm wall has been constructed in a medium-stiff Central Jakarta clay. Measurements on wall deflections were made during the construction. The numerical simulations were conducted by using a hypoplasticity model (HC model) for clays which is capable of modeling small strain non-linearity, soil anisotropy, and recent stress-history effects. Properties of the medium-stiff Jakarta clay were collected and studied carefully to calibrate the HC model. Numerical simulations with consideration of pre-excavation recent stress history effect is thus suggested herein and parameters of HC model used for excavations in Central Jakarta are thus recommended also.

## 1. INTRODUCTION

Jakarta is a rapidly developing megacity that demands to maximize the use of underground space. More and more large deep excavations are under construction and their deformations will affect adjacent infrastructures such as buildings, road, bridges, and public utilities. To properly estimate the interactions among the affected soil, excavation support system and adjacent structures in these projects, advanced soil constitutive models must be used to represent soil behavior during design. Features of soil behavior that affect the calculation of ground movements including soil nonlinearity at very small strains, stiffness anisotropy, soil compressibility and recent stress history effects should be well simulated in the soil model.

A non-symmetric excavation in Central Jakarta was used as a case history. A 3.1 m height of embankment with width about 66 m was located at one side of the excavation. The construction of the embankment altered the stress-history of soils subjected to excavation activities later. The so-called recent stress history effect is defined as the pre-excavation events that generated the current state of effective stresses of the clays. The effect of recent stress history of soils have been studied mostly at the laboratory scale for London clay (Atkinson et al. 1990), Bothkennar clay (Smith et al. 1992), Boston blue clay (Santagata et al. 2005), and Chicago clays (Cho 2007, Finno and Kim 2012). Significant differences on soil stiffness in the small strain range were found as a result of those experimental programs, and it was concluded that the observed soil responses depends on the recent stress history of the material prior to shearing.

An advanced soil constitutive model, hypoplasticity model for clays (HC model) developed by Masin (2005, 2013 and 2014), is adopted in this study. HC model is capable of capturing the features that represent the small strain stiffness of soils, stiffness anisotropy and recent stress-history effects. (Arboleda et al 2017, Teng et al. 2018). Numerical simulations of the hypothetical excavation made through the Central Jakarta clays are presented to illustrate the effect of pre-excavation recent stress history effects on the computed ground movements. The performance of HC model, with well-calibrated parameters, on the magnitude and distribution of the computed excavation-induced ground movements is presented herein.

## 2. PROJECT BACKGROUND

Soil in Jakarta is generally composed by quaternary and tertiary deposit (Firmansyah & Sukamta 2000). Quartenary deposit formed by volcanic ash which divided into 3 layers: 3-5 m thick of upper lahar; alternate silty clay, silty sand and sandy silt; and about 5 m thick of lower lahar that consists of cemented silty sand. Tertiary deposit is located 35 m below the ground surface. This layer consists of a very thick (more than 100 m) greenish silt with consistency from very stiff to hard. Laboratory test results of Jakarta clay such as index properties, oedometer tests, consolidated undrained tests and seismic down-hole test had been taken. Field measurement of wall deformation is also collected. Soil properties for Central Jakarta clay at the site are shown in Figure 1.

The depth of the excavation is 24.85 m, with 1.2 m thick and 33.7 m deep of diaphragm wall. The groundwater level was at a depth of 2.8 m below the ground surface (GL-2.8 m). A road embankment with total length 66 m is located at one side of embankment. Figure 2 shows the excavation profile.

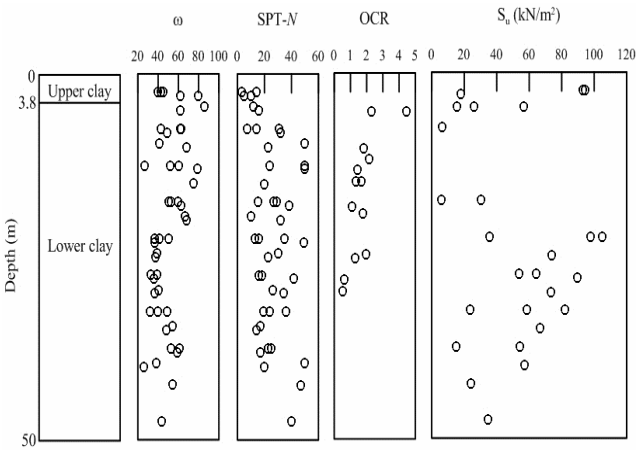


Figure 1. Soil properties

## 3. SOIL PARAMETER

The basic hypoplasticity model have 5 parameters: $\phi$', $\lambda^*$, $\kappa^*$, N and $\upsilon_{pp}$. These parameters are similar to parameters used in Modified Cam Clay model. The model is not based on a conventional elastoplastic framework decomposing strains in elastic and plastic components, and consequently does not involve complex yield-surface and plastic-potential definitions. It captures the nonlinear behavior of soils at large strains in the framework of critical-state soil mechanics by means of the Matsuoka-Nakai shape of the critical-state locus in stress space. HC model used herein is enhanced by intergranular strain concept which can represent the soil behavior at small strain. Since this model is using critical soil mechanic concept, the friction angle is determined by stress at critical state. There are 9 additional soil parameters for intergranular strain parameter: $\alpha_G$, $\alpha_E$, $\alpha_\upsilon$, $A_g$, $n_g$, $m_{rat}$, R, $\beta$r, and $\chi$. Table 1 summarized the parameters of the hypoplasticity model for clays.

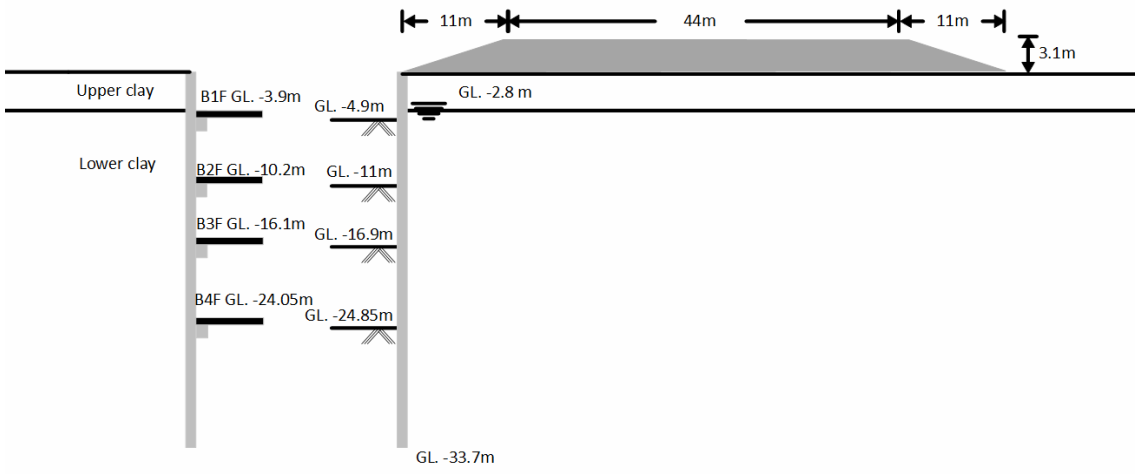


Figure 2. Excavation profile

Table 1. Parameters for HC model

| No. | Symbol | Parameter name |
|---|---|---|
| 1 | N | Position of normal compression line |
| 2 | $\lambda^*$ | Slope of normal compression line |
| 3 | $\kappa^*$ | Slope of unloading line |
| 4 | $\phi$' | Critical-state friction angle |
| 5 | $\upsilon_{pp}$ | Stiffness fitting parameter |
| 6 | $\alpha_G$,$\alpha_E$,$\alpha_\upsilon$ | Anisotropy coefficient of shear, Young and Poisson's moduli |
| 7 | $A_g$ | Stress dependency of $G_{vh}$ on mean |
| 8 | $n_g$ | normal stress |
| 9 | $m_{rat}$ | Very small strain behaviour upon strain path reversals |
| 10 | R | Size of elastic range |
| 11 | βr | Material constant controlling the rate of evolution of the intergranular strain tensor |
| 12 | χ | Material constant controlling the rate of degradation of the shear stiffness |
| 13 | OCR | Over consolidated Ratio |

Since available data for Central Jakarta Clay at small strain level is limited, some parameters were evaluated from several references (as listed in Table 3). $\alpha_G$ is set to be 1 to ignore the anisotropy behavior. The parameter $m_{rat}$ is an intergranular strain parameter that controls the very small strain behavior of clays upon strain path reversals. A value of 1 is chosen for this parameter as a material independent constant and the very small shear stiffness was controlled with the parameters $A_g$ , $n_g$ and the remaining three intergranular strain parameters (Arboleda et al 2017). R as size of elastic range was taken equal to 5E-5 (Masin 2014). In fact, Central Jakarta Clay could be further categorized into 2 layers: upper clay and lower clay. Some parameters calibrated in this simulation mainly focus on lower clay layer because this layer dominates to wall deformation. Table 2 summarized parameters used in this study.

Table 2. parameter of Central Jakarta Clay for HC model

| No. | Symbol | Upper clay | Lower clay | Source |
|---|---|---|---|---|
| | | Value | | |
| 1 | N | 1.52 | 1.285 | Oedometer tests |
| 2 | $\lambda^*$ | 0.126 | 0.098 | Oedometer tests |
| 3 | $\kappa^*$ | 0.018 | 0.011 | Oedometer tests |
| 4 | $\phi$' | 38 | 39 | CU tests |
| 5 | $\rho_t$ | 15 | 5 | Optimization from CU test |
| 6 | $\upsilon_{pp}$ | 0.1 | 0.1 | (Masin 2014) |
| 7 | $\gamma$ | 15.46 | 16.67 | Test data |
| 8 | $e_0$ | 1.81 | 1.62 | Test data |
| 9 | $\alpha_G$ | 1 | 1 | Assumed value |
| 10 | $A_g$ | 15500 | 15500 | Downhole tests |
| 11 | $n_g$ | 0.46 | 0.46 | Downhole tests |
| 12 | $m_{rat}$ | 1 | 1 | (Arboleda et al 2017) |
| 13 | R | 5E-05 | 5E-05 | (Masin 2014) |
| 14 | βr | 0.08 | 0.08 | (Masin 2014) |
| 15 | χ | 0.9 | 0.9 | (Masin 2014) |
| 16 | OCR | 6.25 | 3.37 | Optimization from CU test |

### 3.1 Parameter $\lambda^*$,$\kappa^*$, and N

Thirteen oedometer test results around excavation site were collected to determine $\lambda^*$,$\kappa^*$, N and OCR. $\lambda^*$,$\kappa^*$, N are obtained from ln(1+e) vs ln p space from oedometer test results. $\lambda^*$ and , $\kappa^*$ are slope of normal compression line and unloading line respectively as shown in Figure 3.

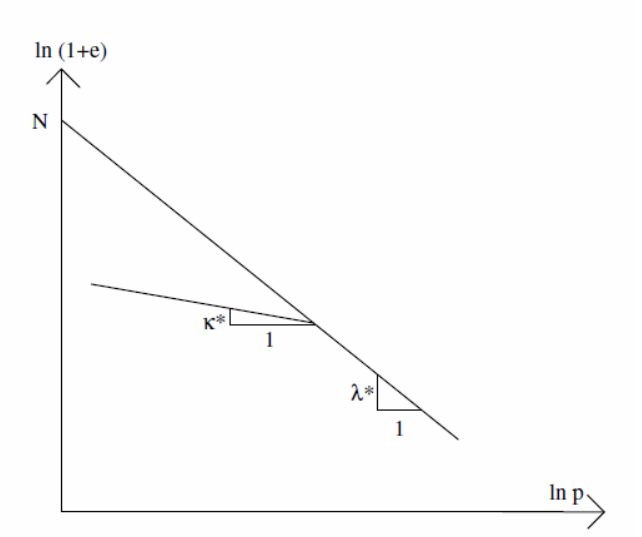


Figure 3. Definition of parameters N, $\kappa^*$ and $\lambda^*$

In order to evaluate the sampling disturbance, specimen quality designation (SQD) value of 13 oedometer data results were calculated by method propose by Terzaghi et al. (1996). This method proposed volumetric strain measured at $\sigma'_{v0}$ during oedometer test as a criteria for determining SQD value. Figure 4 shows SQD calculated for these data. SQD result shows poor result, around D to E. Based on recommendation proposed by Terzaghi et al. (1996), soil samples with SQD in range D to E would not produce reliable estimates of $\sigma'_p$ . Poor SQD value will result in decreasing $\sigma'_p$ .

Oedometer test data with volumetric strain at $\sigma'_{v0}$ below 10 was chose to determine $\lambda^*$,$\kappa^*$, and N parameter used in this simulation. From data chosen with SQD below 10, parameter $\lambda^*$,$\kappa^*$, and N are determined by average value for each layer. Figure 5 a, b, c, d shows the figure of various data of $\lambda^*$,$\kappa^*$, N and OCR versus depth.

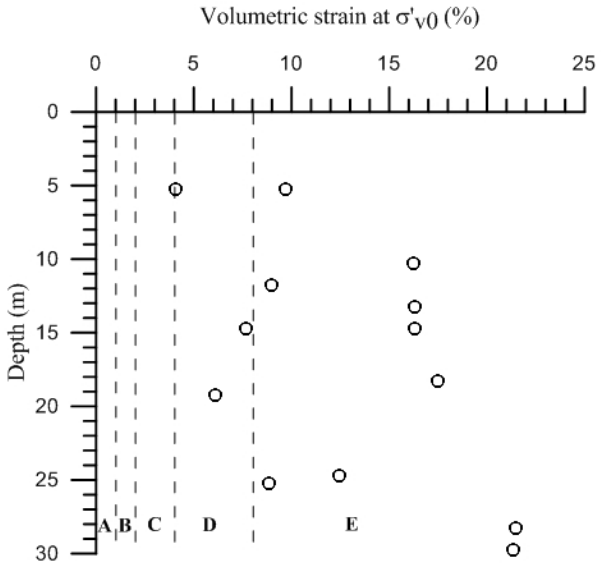


Figure 4. Volumetric strain at ($\sigma'_{v0}$) vs. Depth for specimen quality designation (SQD)

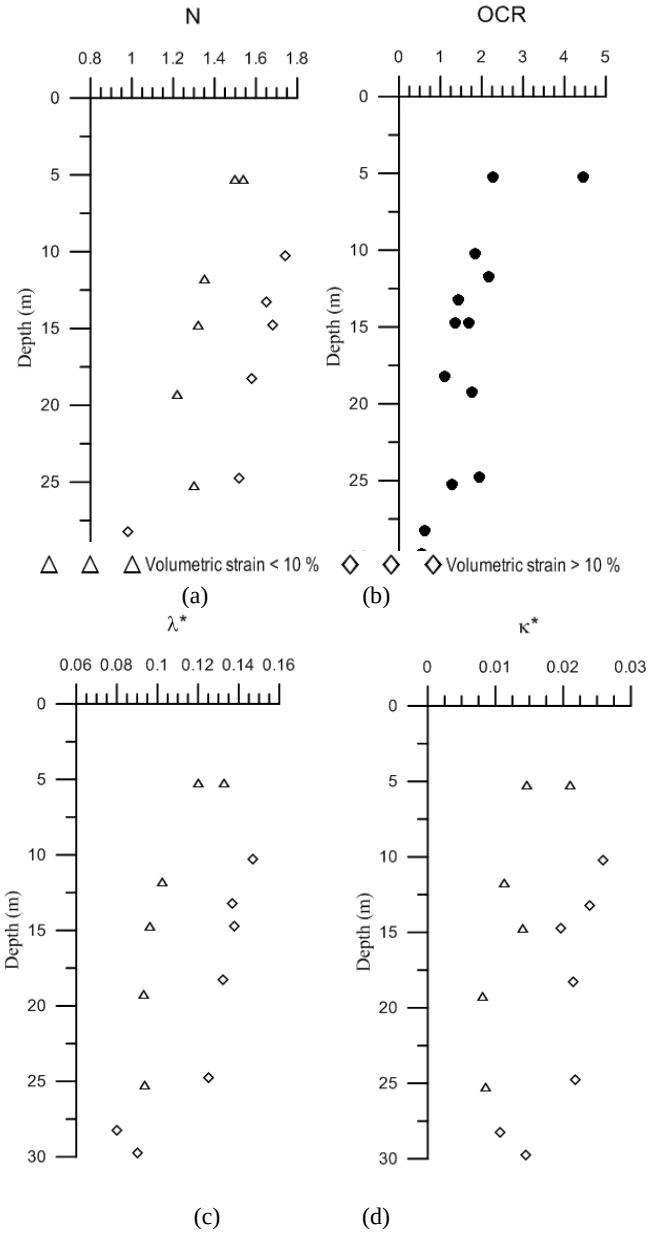


Figure 5. Oedometer test results

### 3.3 Parameter ϕ' and $\rho_t$

CU test results were collected and used to determine values of ϕ', $\rho_t$ and over consolidated ratio (OCR) parameter. ϕ' is friction angle at critical state. $\rho_t$ is shift of mean stress due to cohesion.

For upper clay layer, ϕ'=38$^o$ and $\rho_t$ =15 are used in this simulation based on CU test result. The critical state friction angle for upper soil layer is high. This value shows even for upper clay layer, the soil characteristic is a stiff clay layer. From oedometer test result, OCR for upper clay layer is equal to 3.37. Lower clay layer is a stiff clay soil with used parameters are ϕ'=39$^o$, $\rho_t$ =5 and OCR=6.25. OCR for lower clay layer is higher than obtained from oedometer test result. This value was adopted because it has good alignment with calibration result using HC model which will be explained in section 3.6.

### 3.4 Parameter $A_g$ and $n_g$

Parameter $A_g$ and $n_g$ define the stress dependency of $G_{vh}$ on mean normal stress as proposed by Masin (2014):

$$G_{vh} = p_a A_g \left(\frac{p'}{p_a}\right)^{n_g} \quad (1)$$

where $p_a$= reference pressure parameter (1 kPa), $G_{vh}$ = very small shear modulus in which the double indices refer to the propagation direction and polarization of a shear wave, and $p'$=mean stress. Figure 6 shows range of $G_{vh}/p_a$ vs. $p'/p_a$ from down-hole seismic test result. $A_g$ and $n_g$ are determined according to the regression line.

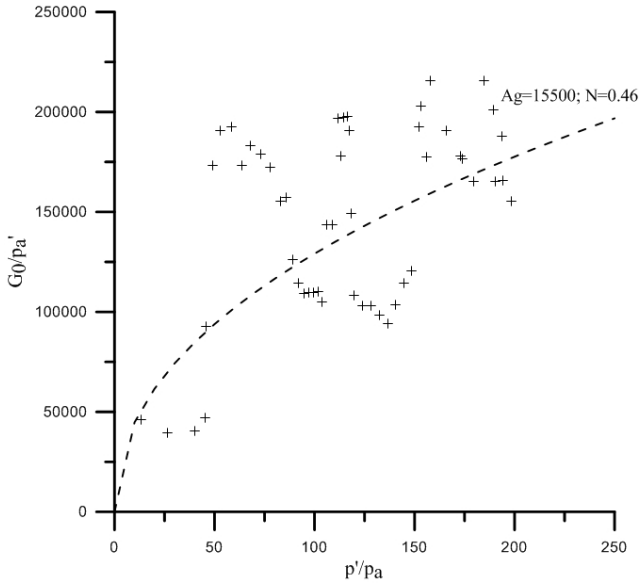


Figure 6. Down-hole seismic test result (Shear modulus at small strain vs. mean stress in terms of reference pressure)

### 3.5 Parameter βr and χ

βr is material constant controlling the rate of evolution of the intergranular strain tensor. χ is material constant controlling the rate of degradation of the shear stiffness. These parameters is usually calibrated by optimisation of CU test. βr and χ in this simulation are 0.08 and 0.9, respectively. These values were suggested by Masin (2014) for stiff clays.

### 3.6 Calibration of Oedometer and CU test result

Fig 4. Shows one oedometer calibration simulation for $\lambda^*$,$\kappa^*$, and N. The purpose of this calibration is to confirm HC model represent the same soil behavior with laboratory test result. One calibration result of oedometer test shown in Figure 7 has good agreement with laboratory test result.

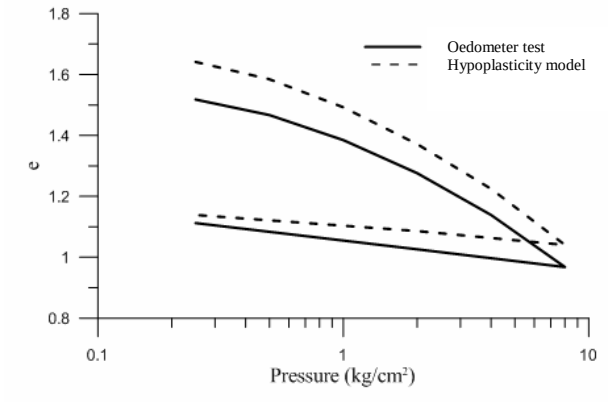


Figure 7. Comparison of oedometer test results with computations from HC model

Central Jakarta clay was formed primarily from volcanic ash. This soil type shows very strong structure even with no history that soil has been subjected to high overburden pressures in the past. A clay layer formed by volcanic ash in New Zealand (Jacquet 1990) shows a high OCR values around 17. Wallace (1993) and Millar (1986) proposed the chemical composition (Iron oxide) of clay may play an important role to the OCR value. Based on the calibration of CU test, a OCR of 6.25 was obtained to yield a reasonable undrained shear strength for Central Jakarta clay. Figure 8 shows the comparison of CU test between laboratory test result and simulation result.

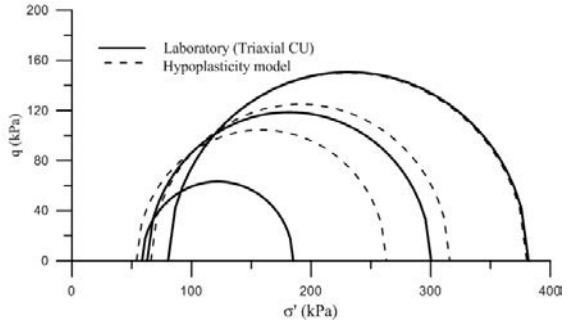


Figure 8. Comparison of CU test result for lower clay layer from laboratory and HC model

## 4. NUMERICAL MODEL OF EXCAVATIONS

In this excavation simulation, soil layers were divided into 2 soil layers. The upper clay, from ground surface level (GL) 0.0 m to GL -3.8 m is a stiff clay layer with $\phi'=38^o$. The lower clay layer, from GL -3.8 m to GL -65m, is a very stiff clay layer with $\phi'=39^o$. There are 11 phases in this simulation as listed in Table 3. Excavation zone is located right next to a 3.1m height of road embankment with width is about 66 m. This road embankment is later connected to a bridge. Because the embankment was built for transportation purpose, the original form of embankment area is assumed as a horizontal ground surface which later is loaded and consolidated by this embankment. This road embankment is located at central Jakarta that had been built over decades. The construction of this embankment is expected has a recent stress history effect to the wall movement. In this simulation, the embankment is consolidated for 20 years in order to make the excess pore pressure fully dissipated. This consolidation step is followed by the installation of the diaphragm wall and four excavation stages.

Table 3. Stage construction

| Phase | Stage Construction |
|---|---|
| 0 | Initial phase |
| 1 | Consolidation of embankment for 20 years |
| 2 | Install diaphragm wall |
| 3 | Excavate to GL. -4.9m (1st excavation stage) |
| 4 | Install B1F at GL. -3.9m |
| 5 | Excavate to GL. -11m (2nd excavation stage) |
| 6 | Install B1F slab at GL. -10.2m |
| 7 | Excavate to GL. -16.9m (3rd excavation stage) |
| 8 | Install B2F slab at GL. -16.1m |
| 9 | Excavate to GL. -24.85m (4th excavation stage) |
| 10 | Install bottom slab GL. -24.05m |

Finite element mesh of the excavation case is shown in Figure 9. Dimension of numerical model in horizontal and vertical are 247 m and 65 m, respectively. The excavation width is 20.5 m. The embankment is symmetry with total length and height of embankment are 66 m and 3.1 m. The height of embankment inclines from zero to 3.1 m with horizontal length equal to 11 m from excavation side. The left boundary is at a distance of 80 m

from the diaphragm wall and the right boundary is at a distance of 80 m from the end of embankment. The left and right vertical boundaries were restrained from horizontal movement and the bottom was restrained from both of the vertical and horizontal movements.

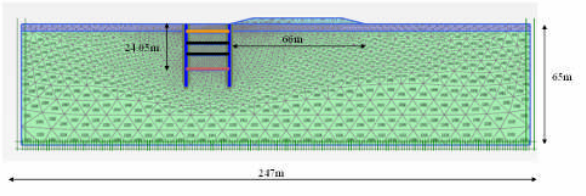


Figure 9. Finite element mesh of excavation case at Central Jakarta

The stiffness of structural parameters is reduced by 20%, considering that the stiffness of the concrete retaining wall reduces
when subjected to large bending moment of diaphragm wall causes the occurrence of the crack in the concrete. The axial stiffness of the concrete floor slabs is also reduced by 20%. Table 4 contains material properties of structures used in numerical simulation and t, E and υ means thickness, elastic modulus and Poisson ratio.

Table 4. Material properties of structures

| Structure | Type | t (m) | E (Mpa) | υ |
|---|---|---|---|---|
| B1F | slab | 0.8 | 21000 | 0.15 |
| B2F | slab | 0.4 | 21000 | 0.15 |
| B3F | slab | 0.4 | 21000 | 0.15 |
| B4F | slab | 1 | 21000 | 0.15 |
| D-Wall | wall | 1.2 | 21000 | 0.15 |

## 5. NUMERICAL SIMULATION RESULTS

Wall deflections induced by excavation were monitored by inclinometers. Correction of inclinometer data result had been done as suggested by Hsiung & Hwang (2009). The inclinometer reading can be trusted once the tip of inclinometer properly embedded into a stable stratum to avoid the inclinometer tip move together with diaphragm wall. Corrections had been calculated by using B1F slab as referred point at first excavation stage. Other inclinometers data at B1F slab which move inward to excavation zone after first excavation stage had been moved fit to the reference point.

At no-embankment side, corrected maximum deformation of diaphragm wall based on inclinometer data result at final excavation stage after completion of slab and 1 month after are 25 mm and 42 mm, respectively. At embankment side, corrected maximum deformation of diaphragm wall at final excavation stage after completion of slab and 1 month after are 22 mm and 45 mm, respectively. Figure 10 shows wall deflection of simulation result and field measurement at no-embankment side. Wall deformation of simulation result at first excavation stage show slightly different with field measurement while at second and third excavation stages show good agreement with field measurement. For last exacavation stage, there is deformation difference between deformation at completion of slab and 1 month after completion of slab. Maximum wall deformation of simulation result is 33 mm.

Figure 11 show inclinometer data result and simulation result of embankment side of diaphragm wall. Wall deformation at 1st excavation stage shows slightly deformation difference to field measurement. For 2nd and 3rd excavation stages, maximum wall deformations of simulation result are 5-7 mm larger than field measurement. Maximum wall deformation at final stage is 43 mm.

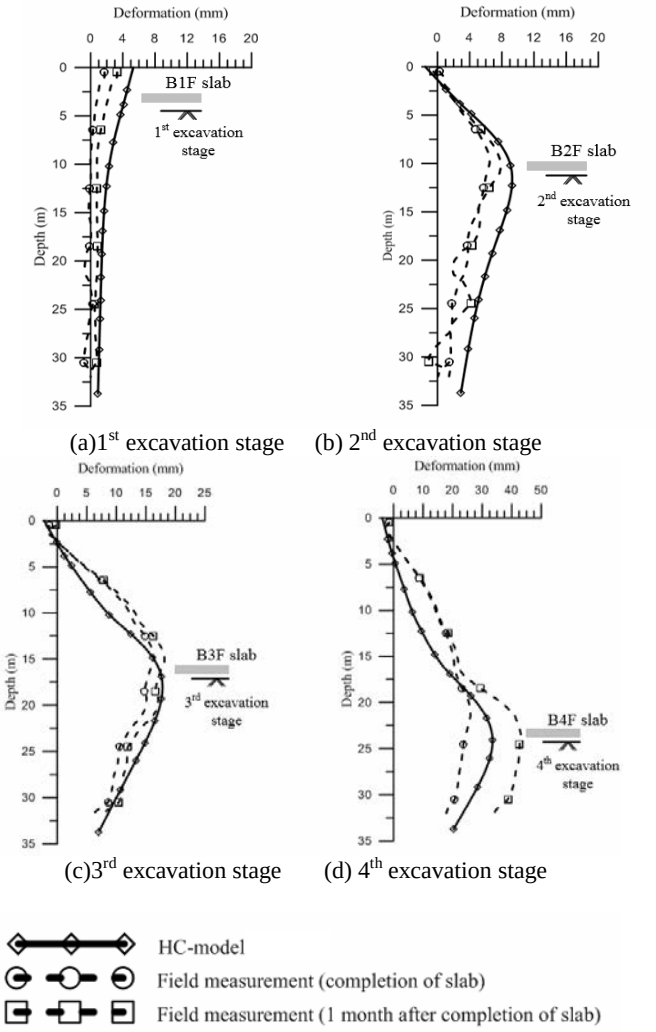


(a)1st excavation stage (b) 2nd excavation stage

(c)3rd excavation stage (d) 4th excavation stage

Figure 10. Deformations of diaphragm wall at no-embankment side at various stages

Maximum wall deformation from simulation result of final excavation stage at embankment side is larger around 10 mm than that at no-embankment side. The possible reason is even the embankment has already been consolidated for 20 years and excess pore pressure calculated in simulation is very small, under 1kPa, the embankment load still has an effect to wall deformation. It is aware that a significant difference is seen in the aspect of lateral wall movement measured for the time after the completion of B4F slab and 1 month after and the reason has to be further explored in the future.

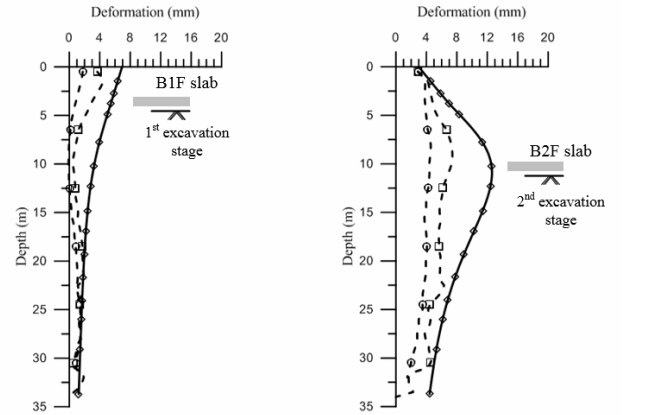


(a)1st excavation stage (b) 2nd excavation stage

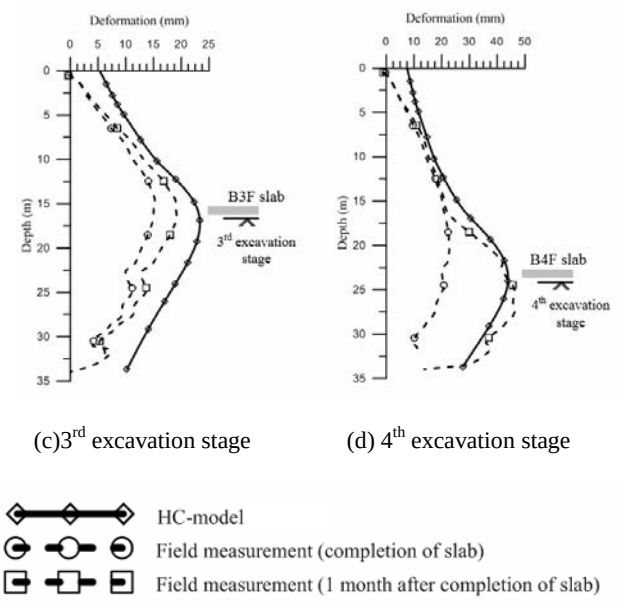


(c)3rd excavation stage (d) 4th excavation stage

Figure 11. Deformations of diaphragm wall at embankment side at various excavation stages

## 6. CONCLUSION

Based on laboratory data, field measurement collected and finite element analyses, the conclusions of this study are as following:

1. Oedometer test results show that: the range of $\lambda^*$ for Central Jakarta Clay is from 0.08 to 0.16; $\kappa^*$ is in a range of 0.005 to 0.025; N is in a range of 1.2 to 1.6. Actually, Central Jakarta Clay could be further categorized into 2 layers: upper clay and lower clay.
2. Calibration of CU test show good agreement with $\phi'=39^o$ for lower clay layer. This indicates that lower clay layer is a stiff clay layer with high friction angle. From this calibration, it is also indicated OCR for lower clay layer is at high value, equal to 6.25 in consideration of volcanic structure.
3. The deformation analysis of diaphragm wall due to excavation histories have a better agreement at earlier excavation stages. Simulation on pre-excavation activity by advanced HC model is applicable to Central Jakarta Clay and yield a good simulation results.
4. Research about small strain behavior in Indonesia is still limited. As a pioneer study for HC model on Central Jakarta Clay, this study provides a range for parameters. Further research in small strain behavior is highly demanded for the advanced soil model.

## 7. REFERENCES

Arboleda-Monsalve L. G., Teng F.-C., Kim T. and Finno R. (2017). "Numerical Simulation of Triaxial Stress Probes and Recent Stress-History Effects of Compressible Chicago Glacial Clays." *J. Geotech. Geoenv. Eng.*, 10.1061/(ASCE)GT.1943-5606.0001684, 04017029

Atkinson, J. H., Richardson, D., and Stellabrass, S. E. (1990). "Effect of recent stress history on the stiffness of overconsolidated soil." *Geotechnique*, 40(4), 531-540

Cho, W., (2007). "Recent stress history effects on compressible Chicago glacial clay." Ph.D. thesis, Northwestern Univ., Evanston, IL.

Finno, R. J., and Kim, T. (2012). "Effects of stress path rotation angle on small strain responses." *J. Geotech Geoenviron. Eng*., 10.1061/(ASCE)GT.1943-5606.0000612, 526-534

Firmansyah, I., & Sukamta, D. (2000). Common Practice Basement Construction in Jakarta-Indonesia. *ACF Symposium Technical Report*, 28-39.

Hsiung, B. B. C., & Hwang, R. N. (2009). Correction of inclinometer readings for movement at tips. *Geotechnical Engineering*, 40(2), 39-48.

Jacquet, D. (1990). Sensitivity to remoulding of some volcanic ash soils in New Zealand. *Engineering Geology*, 28, 1-25

Masin, D. (2005). A hypoplastic constitutive model for clays. *International Journal for Numerical and Analytical Methods in Geomechanics*, 29(4):311-336

Masin, D. (2013). "Clay hypoplasticity with explicitly defined asymptotic states." *Acta Geotechnica*, 8(5), 481-496

Masin, D. (2014). "Clay hypoplasticity model including stiffness anisotropy." *Geotechnique*, 64(3), 232-238

Millar, P. 1986 Taranski Brown Ash A Discussion on the Influence of Iron Oxide Bonding on Engineering Performance Ministry of Works and Development, Central Laboratories, Report No. 2-86/8

*PLAXIS 2D* [Computer software].

Santagata, M., Germaine, J. T., and Ladd, C. C. (2005). "Factors affecting the initial stiffness of cohesive soils." *J. Geotech. Geoenviron. Eng*., 10.1061/(ASCE)1090-0241(2005)131:4(430), 430-441

Smith, P. R., Jardine, R. J., and Hight, D. W. (1992). "The yielding of Bothkennar clay." *Geotechnique*, 42(2), 257-274

Teng F.-C., Arboleda-Monsalve L. G., Teng F.-C., and Finno R. (2018). "Numerical Simulation of recent stress-history effects on excavation responses in soft clays." *J. Geotech. Geoenv. Eng.*, 10.1061/(ASCE)GT.1943-5606.0001921

Terzaghi, K, Peck, R. B., & Mesri, G. (1996). *Soil mechanics in engineering practice* (3rd ed.). New York: Wiley.

Wallace, K.B. (1973). "Structural behavior of residual soils of the continually wet Highlands of Papua New Guinea." *Geotechnique*, 23, 471-494